

Long-Horizon Direct Model Predictive Control for Power Converters With State Constraints

Raphael Keusch, Hans-Andrea Loeliger, *Fellow, IEEE*, and Tobias Geyer, *Fellow, IEEE*

Abstract—The paper explores a new approach to model predictive control where both discrete-level input constraints and state constraints are expressed in terms of Gaussian variables with unknown variances. The computations boil down to repeating Kalman-type recursions, with linear complexity in the prediction horizon. In consequence, the proposed approach can handle long prediction horizons with both discrete-level input constraints and state constraints, which has been a largely unresolved problem. The paper demonstrates and evaluates the application of this approach by applying it to the control problem of a three-level power converter with an LC filter. In this application, long horizons are mandatory in order to obtain low harmonic current distortions, and certain state constraints must be imposed to prevent damage to the converter. The proposed controller can easily handle 100 or more time steps and is shown to perform remarkably well, not only in steady-state, but also in transients and in case of a phase-to-ground fault.

Index Terms—Finite-control-set model predictive control (FCS-MPC), control as inference, normals with unknown variance (NUV), Gaussian message passing

I. INTRODUCTION

DIRECT model predictive control (MPC) schemes, which directly control the semiconductor switches of power converters, have recently received significant attention [1], [2]. Particularly promising is finite-control-set MPC (FCS-MPC), which was first proposed in [3] and [4] with a prediction horizon of one step and exhaustive enumeration to solve the underlying optimization problem. For first-order systems, such as inductive loads, the steady-state performance in terms of harmonic current distortions and switching frequency is similar to that of classic linear controllers with carrier-based pulse width modulation (CB-PWM) [5], provided that certain design rules are adhered to [6].

For higher-order systems such as converters with LC filters, long prediction horizons are vital to achieve low current distortions at acceptable switching frequencies. In the setting of [7], simulation results indicate that the prediction horizon should be at least 0.5 ms, which (for a sampling interval of 25 μ s) translates to 20 time steps. In [7], the resulting computational problem was eased by increasing the sampling interval to 125 μ s, which made the optimization tractable by a

branch and bound method called sphere decoding [8], [9], but has a detrimental effect on the harmonic current distortions.

During transients, the high bandwidth of FCS-MPC tends to produce pronounced spikes in the electrical converter quantities. In particular the converter currents and the filter capacitor voltages tend to exceed their nominal values by a factor of up to two [7]. Such high currents and voltages lead to a trip of the converter system or even to its damage. To prevent this, constraints should be imposed on these state variables. Solving the optimization problem underlying FCS-MPC with state constraints is straightforward in case of exhaustive enumeration [10], but doing so with sphere decoding remains a largely unresolved problem, see [11] for a first attempt.

An alternative approach is for the controller to manipulate the switching instants of a pre-computed switching pattern, such as an optimized pulse pattern [12]. A small-signal linearization around the nominal switching instants leads to a quadratic program, which is computationally relatively easy to solve and to which state constraints can be added [13]. Another alternative is to employ indirect MPC, i.e., MPC with a subsequent PWM stage. Indirect MPC is rarely considered in the literature, but state constraints can be added relatively easily, as shown, for example, in [14].

In this paper, we propose an entirely different approach: we work with a linear-Gaussian state space model, where constraints are expressed in terms of Gaussian “priors” with unknown means and variances.

Expressing non-Gaussian variables in terms of Gaussians with unknown parameters is not a new idea: on the one hand, expressing sparsifying priors as normals with unknown variances (NUV) is the key idea of sparse Gaussian learning [15]–[18]; on the other hand, the idea is closely related to variational representations of cost functions as in [19], [20]. In this paper, we specifically use composite-NUV representations of two-level constraints as in [21], [22] and of half-space constraints as in [23].

We also note that the approach of this paper may be viewed as an example of control by inference [24]–[27].

The combination of NUV representations of priors or constraints with linear state space models is particularly attractive as it leads to iterative algorithms with a complexity that is linear in the length of the prediction horizon [21], [22]. In consequence, the approach of this paper can easily handle long horizons of 100 time steps and more. The approach is not guaranteed to find the best solutions of the underlying optimization problems, but empirically, it produces very good solutions. In any case, the ability to use long horizons and

R. Keusch and H.-A. Loeliger are with the Department of Information Technology and Electrical Engineering, ETH Zurich, 8092 Zurich, Switzerland (e-mail: keusch@isi.ee.ethz.ch, loeliger@isi.ee.ethz.ch).

T. Geyer is with ABB System Drives, 5300 Turgi, Switzerland (e-mail: t.geyer@ieee.org)

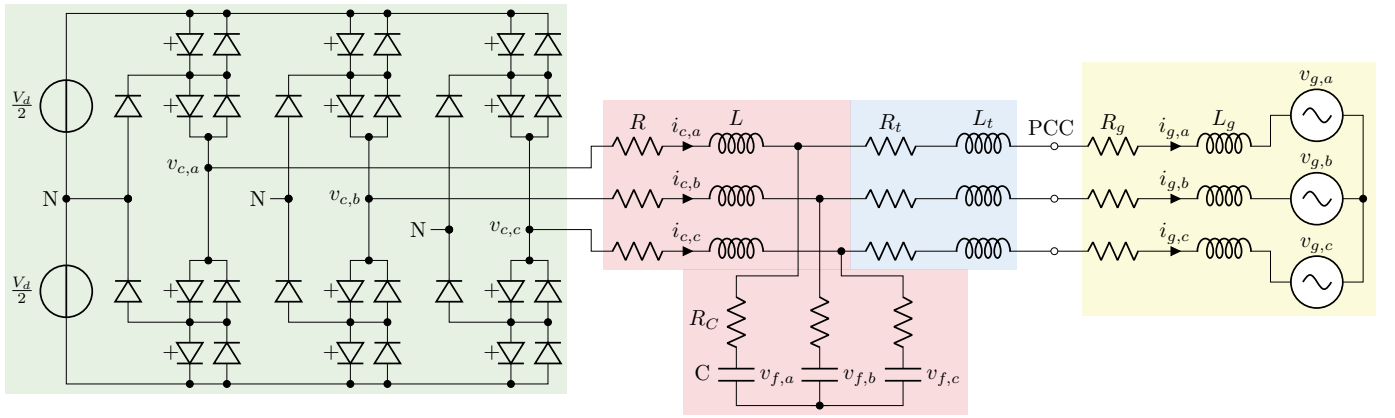


Fig. 1. Electrical circuit of the grid-connected converter. The left part illustrates the neutral-point clamped converter (green), followed by the LC filter (red), the transformer (blue) and the grid (yellow).

to impose versatile state constraints far outweighs the lack of optimality.

Conceptually and mathematically, the approach of this paper was proposed in [21]–[23]. However, this paper is the first to apply this approach to a real-world control problem. Consequently, we will not, in this paper, rederive the pertinent NUV representations and algorithms, but we will describe their application in sufficient detail for independent implementation and verification.

The paper is structured as follows. In Section II, a linear state space representation of the converter model is derived. In Section III, the underlying control problem is formulated and the proposed control algorithm is described. In Section IV, the performance of the proposed control algorithm is evaluated, where steady-state operation, transient operation, and a phase-to-ground fault are examined.

The following notation will be used. The identity matrix of dimension n is denoted by I_n and the all-zero matrix of dimension $n \times m$ is denoted by $0_{n \times m}$. A (block-)diagonal matrix with diagonal elements a_1, \dots, a_n is denoted by $\text{diag}(a_1, \dots, a_n)$. The Gaussian probability density function in x with mean m and covariance matrix V is denoted by $\mathcal{N}(x; m, V)$. The superscript (i) is used to represent the iteration index of an iterative algorithm, e.g., $\theta^{(i)}$ identifies the parameter θ in the iteration i . The discrete-time counterpart of a continuous-time quantity $x(t)$ is denoted by x_k .

II. STATE SPACE MODEL

We will work with a medium-voltage converter system that is rated at 9 MVA and operates at a switching frequency of a few hundred Hertz; however the results are directly applicable also to low-voltage converters operating in the kilo Hertz range.

Consider the grid-connected converter shown in Fig. 1. The three-phase neutral-point clamped (NPC) converter is connected via an LC filter and a transformer to a point of common coupling (PCC). The grid is modeled by a grid impedance and a grid voltage. The mathematical modeling of the physical system follows [13, Section 3.3.1], with an additional augmentation of the state-space model in preparation for Section III-D.

To map quantities between the three-phase abc system and the stationary orthogonal $\alpha\beta$ reference frame, we use the reduced Clarke transformation [28] $\xi_{\alpha\beta} = P\xi_{abc}$ and its inverse $\xi_{abc} = P^\dagger\xi_{\alpha\beta}$, respectively, where $\xi_{abc} = [\xi_a \ \xi_b \ \xi_c]^\top$ is a vector in the abc system and $\xi_{\alpha\beta} = [\xi_\alpha \ \xi_\beta]^\top$ is a vector in the $\alpha\beta$ reference frame. The transformation matrices are defined as

$$P \triangleq \frac{2}{3} \begin{bmatrix} 1 & -\frac{1}{2} & -\frac{1}{2} \\ 0 & \frac{\sqrt{3}}{2} & -\frac{\sqrt{3}}{2} \end{bmatrix}, \quad \text{and} \quad P^\dagger \triangleq \begin{bmatrix} 1 & 0 \\ -\frac{1}{2} & \frac{\sqrt{3}}{2} \\ -\frac{1}{2} & -\frac{\sqrt{3}}{2} \end{bmatrix}. \quad (1)$$

Furthermore, it is convenient to normalize all quantities using a per-unit system. Its base values and the system parameters will be defined in Section IV-B.

A. Physical Model

The (total) DC-link voltage $V_d \in \mathbb{R}$ is assumed to be constant and the converter's neutral point potential is fixed to zero. The converter output voltage of each phase can take on the three voltage levels $\{-\frac{V_d}{2}, 0, \frac{V_d}{2}\}$, depending on the switching state of the respective phase. The converter voltage is consequently defined as

$$\begin{bmatrix} v_{c,a}(t) \\ v_{c,b}(t) \\ v_{c,c}(t) \end{bmatrix} \triangleq \frac{V_d}{2} \begin{bmatrix} u_a(t) \\ u_b(t) \\ u_c(t) \end{bmatrix}, \quad (2)$$

where $u(t) \triangleq [u_a(t) \ u_b(t) \ u_c(t)]^\top$ is the three-phase switch position with $u(t) \in \{-1, 0, 1\}^3$. The converter voltage in the $\alpha\beta$ reference frame is

$$v_{c,\alpha\beta}(t) = \begin{bmatrix} v_{c,\alpha}(t) \\ v_{c,\beta}(t) \end{bmatrix} = P \begin{bmatrix} v_{c,a}(t) \\ v_{c,b}(t) \\ v_{c,c}(t) \end{bmatrix}. \quad (3)$$

The grid voltage is given by

$$v_{g,\alpha\beta}(t) \triangleq \sqrt{\frac{2}{3}} V_{g,LL} \begin{bmatrix} \sin(\omega t) \\ \cos(\omega t) \end{bmatrix}, \quad (4)$$

where $V_{g,LL} \in \mathbb{R}$ denotes the line-to-line root mean square (RMS) grid voltage, and $\omega \in \mathbb{R}$ is the angular fundamental frequency of the grid. Furthermore, we introduce in

with $w_k \triangleq [w_{k,1} \ \cdots \ w_{k,6}]^\top \in \{0,1\}^6$ and

$$D \triangleq \begin{bmatrix} 1 & -1 & 0 & 0 & 0 & 0 \\ 0 & 0 & 1 & -1 & 0 & 0 \\ 0 & 0 & 0 & 0 & 1 & -1 \end{bmatrix}. \quad (20)$$

III. CONTROL METHOD

A. Preliminaries

The proposed algorithm works within a standard receding-horizon MPC strategy as illustrated in Fig. 2: in the first planning period, an input sequence $[\hat{u}_1 \ \cdots \ \hat{u}_K]$ is computed, of which only $[\hat{u}_1 \ \cdots \ \hat{u}_M]$ (with $M < K$) are actually applied; in the second planning period, a new input sequence $[\hat{u}_{M+1} \ \cdots \ \hat{u}_{M+K}]$ is computed, of which only $[\hat{u}_{M+1} \ \cdots \ \hat{u}_{2M}]$ are applied; and so on. In the numerical examples (Section IV), we will use $M = 1$.

B. Detailed Problem Description

In the following, we consider only a single planning period with horizon $\mathcal{K} = \{1, \dots, K\}$.

The control scheme addresses several potentially opposing objectives. First and foremost, the controller must determine a ternary input sequence $\hat{u} \triangleq [\hat{u}_1 \ \cdots \ \hat{u}_K]$ (or, equivalently, a binary input sequence $\hat{w} \triangleq [\hat{w}_1 \ \cdots \ \hat{w}_K]$ according to (19)) such that the grid current $\tilde{y}_k = i_{g,\alpha\beta,k}$ tracks the given reference current $\check{y}_k \triangleq \check{y}_{g,\alpha\beta,k} \in \mathbb{R}^2$, i.e., we wish to minimize

$$\sum_{k \in \mathcal{K}} \|\check{y}_{g,\alpha\beta,k} - i_{g,\alpha\beta,k}\|^2 = \sum_{k \in \mathcal{K}} \|\check{y}_k - \tilde{y}_k\|^2. \quad (21)$$

Accurate tracking of the reference currents minimizes the current ripple and, consequently, the harmonic distortions of the grid current. Second, we wish to keep the switching frequency of the semiconductor switches sufficiently low, in order to reduce the thermal stress on the semiconductors and to avoid excessive power losses. Clearly, these two control objectives oppose each other, i.e., reducing the switching frequency decreases the tracking performance.

Moreover, in order to avoid damaging the converter or the LC filter, some electrical quantities of the system must not exceed predefined bounds. In this case study, we require the converter currents and the capacitor voltages to be upper- and lower-bounded (i.e., box-constrained) by

$$i_{c,abc,k} \in [-\delta_i, \delta_i]^3 \quad \text{and} \quad v_{f,abc,k} \in [-\delta_v, \delta_v]^3, \quad (22)$$

for all $k \in \mathcal{K}$ and with bounds $\delta_i, \delta_v \in \mathbb{R}$. In summary, we have the optimization problem

$$\hat{u} = \underset{u}{\operatorname{argmin}} \frac{1}{s^2} \sum_{k \in \mathcal{K}} \|\check{y}_k - \tilde{y}_k\|^2 + \frac{1}{r^2} \sum_{k=2}^K \|u_k - u_{k-1}\|^2 \quad (23a)$$

subject to

$$u_k \in \{-1, 0, 1\}^3, \quad k \in \mathcal{K} \quad (23b)$$

$$i_{c,abc,k} \in [-\delta_i, \delta_i]^3, \quad k \in \mathcal{K} \quad (23c)$$

$$v_{f,abc,k} \in [-\delta_v, \delta_v]^3, \quad k \in \mathcal{K}, \quad (23d)$$

with $u \triangleq [u_1 \ \cdots \ u_K]$, and weight parameters $s^2 > 0$ and $r^2 > 0$.

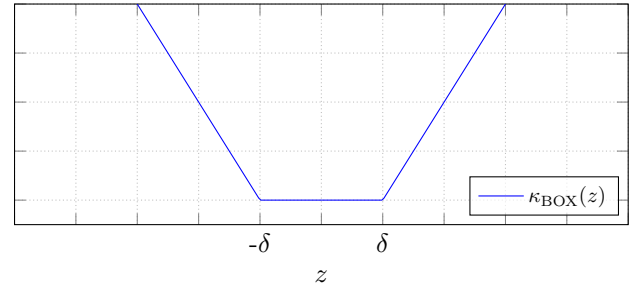


Fig. 4. The penalty function $\kappa_{\text{BOX}}(z)$ in (24) and (25).

Numerical experiments have shown that penalizing the L_1 norm of the level differences in (23a) does not significantly increase the control performance. We thus chose the L_2 norm for reasons of lower computational complexity.

C. Outline of Control Algorithm

We will formulate the constrained optimization problem (23) as an unconstrained statistical estimation problem based on a linear Gaussian model with unknown parameters. In particular, the discrete-level constraints (23b) are handled by binarizing priors as in [21], [22], and the state constraints (23c) and (23d) are handled by box constraint priors as in [23].

The optimization problem is then solved using an iterative algorithm (see Section III-E) that alternates between estimating statistical quantities in a linear Gaussian model (Step 1 in Section III-E) and updating the unknown means and variances (Step 2 in Section III-E), which may be viewed as an instance of iteratively reweighted least squares.

After termination, the first M elements of the computed input sequence \hat{u} (solution of the optimization problem (23)) are used to control the physical system (the converter) for M time steps, cf. Section III-A. A block diagram describing the overall control approach is given in Fig. 3.

D. Statistical Model

We begin by expressing the constraints (23c) and (23d) by the penalty functions (see Fig. 4)

$$\kappa_{\text{BOX}}(i_{c,n,k}) \triangleq \gamma(|i_{c,n,k} + \delta_i| + |i_{c,n,k} - \delta_i|) \quad (24)$$

and

$$\kappa_{\text{BOX}}(v_{f,n,k}) \triangleq \gamma(|v_{f,n,k} + \delta_v| + |v_{f,n,k} - \delta_v|) \quad (25)$$

for $k \in \mathcal{K}, n \in \{a, b, c\}$. Note that γ is a design parameter and needs to be chosen sufficiently large to ensure that (23c) and (23d) hold, cf. Section III-F. The constrained optimization

problem (23) can then be formulated as

$$\begin{aligned} \hat{w} = \operatorname{argmax}_w & \prod_{k \in \mathcal{K}} \exp\left(-\frac{1}{2s^2} \|\check{y}_k - \tilde{y}_k\|^2\right) \\ & \cdot \prod_{k=2}^K \exp\left(-\frac{1}{2r^2} \|u_k - u_{k-1}\|^2\right) \\ & \cdot \prod_{k \in \mathcal{K}} \prod_{n \in \{a,b,c\}} \exp\left(-\kappa_{\text{BOX}}(i_{c,n,k})\right) \\ & \cdot \prod_{k \in \mathcal{K}} \prod_{n \in \{a,b,c\}} \exp\left(-\kappa_{\text{BOX}}(v_{f,n,k})\right) \\ & \cdot \prod_{k \in \mathcal{K}} \prod_{n \in \{1,\dots,6\}} \rho_{\text{BIN}}(w_{k,n}, \theta_{k,n}) \end{aligned} \quad (26)$$

with binary input $w \triangleq [w_1 \ \dots \ w_K]$ as in (19). The factors in line 3 and 4 of (26) are handled by box constraint priors [23] using the NUV representation

$$\exp\left(-\kappa_{\text{BOX}}(z)\right) = \max_{\sigma_a^2, \sigma_b^2} \mathcal{N}(z; -\delta, \sigma_a^2) \rho(\sigma_a^2) \cdot \mathcal{N}(z; \delta, \sigma_b^2) \rho(\sigma_b^2), \quad (27)$$

where $\rho(\sigma^2) \triangleq \sqrt{2\pi\sigma^2} \exp(-\gamma^2\sigma^2/2)$, and σ_a^2 and σ_b^2 are unknown parameters. The factors ρ_{BIN} in line 5 of (26) are binarizing NUV priors as in [21], [22], the discussion of which is beyond the scope of this paper.

With $y \triangleq [y_1 \ \dots \ y_K]$ and $\check{y} \triangleq [\check{y}_1 \ \dots \ \check{y}_K]$, (26) is summarized in a statistical model

$$p(y, w | \check{y}) \propto p(y|w) \prod_{k \in \mathcal{K}} p(w_k) p(\check{y}_k | y_k), \quad (28)$$

where $p(y|w)$ is deterministic according to (15) (with known initial state x_0), $\prod_{k \in \mathcal{K}} p(w_k)$ is the last line of (26), and $\prod_{k \in \mathcal{K}} p(\check{y}_k | y_k)$ subsumes all the other factors in (26). The NUV factors

$$p(w_k) \triangleq \mathcal{N}(w_k; \vec{m}_{W_k}, \vec{V}_{W_k}), \quad (29)$$

have the unknown parameters

$$\vec{m}_{W_k} \triangleq [\vec{m}_{W_{k,1}} \ \dots \ \vec{m}_{W_{k,6}}]^\top, \quad (30)$$

$$\vec{V}_{W_k} \triangleq \operatorname{diag}\left(\vec{\sigma}_{W_{k,1}}^2, \dots, \vec{\sigma}_{W_{k,6}}^2\right), \quad (31)$$

and the NUV factors

$$p(\check{y}_k | y_k) \triangleq \mathcal{N}(y_k; \vec{m}_{Y_k}, \vec{V}_{Y_k}), \quad (32)$$

have the (partially unknown) parameters

$$\vec{m}_{Y_k} \triangleq [\check{y}_{g,\alpha,k} \ \check{y}_{g,\beta,k} \ 0 \ 0 \ 0 \ \vec{m}_{i_{c,a,k}} \ \vec{m}_{i_{c,b,k}} \ \vec{m}_{i_{c,c,k}} \ \vec{m}_{v_{f,a,k}} \ \vec{m}_{v_{f,b,k}} \ \vec{m}_{v_{f,c,k}}]^\top, \quad (33)$$

$$\vec{V}_{Y_k} \triangleq \operatorname{diag}\left(s^2, s^2, r^2, r^2, r^2, \vec{\sigma}_{i_{c,a,k}}^2, \vec{\sigma}_{i_{c,b,k}}^2, \vec{\sigma}_{i_{c,c,k}}^2, \vec{\sigma}_{v_{f,a,k}}^2, \vec{\sigma}_{v_{f,b,k}}^2, \vec{\sigma}_{v_{f,c,k}}^2\right). \quad (34)$$

We denote the set of all unknown parameters by θ , which comprises all \vec{m} 's and $\vec{\sigma}^2$'s on the right-hand-side of (30), (31), (33) and (34), for all $k \in \mathcal{K}$. Note that for fixed θ , the model (28) is entirely Gaussian.

(The arrows over symbols in (29)-(34) and in Table I are consistent with the notation in [21]–[23], [29], where the underlying theory is described.)

TABLE I

STEP 1 OF IAKE IMPLEMENTED BY MBF MESSAGE PASSING WITH INPUT ESTIMATION ASSEMBLED FROM [29].

The algorithm consists of a forward recursion followed by a backward recursion. The former is a standard Kalman filter, but the latter is not quite standard.

Forward recursion for $k = 1, 2, \dots, K$, with $\vec{m}_{X_k} \in \mathbb{R}^{14}$ and $\vec{V}_{X_k} \in \mathbb{R}^{14 \times 14}$, initialized with mean $\vec{m}_{X_0} = x_0$ and covariance matrix $\vec{V}_{X_0} = 0_{14 \times 14}$:

$$\vec{m}_{X_k} = A\left(\vec{m}_{X_{k-1}} + \vec{V}_{X_{k-1}} C^\top G_{k-1} (\vec{m}_{Y_{k-1}} - C \vec{m}_{X_{k-1}})\right) + BD \vec{m}_{W_k} \quad (M.1)$$

$$\vec{V}_{X_k} = A F_{k-1} \vec{V}_{X_{k-1}} A^\top + BD \vec{V}_{W_k} D^\top B^\top \quad (M.2)$$

with

$$G_{k-1} = (\vec{V}_{Y_{k-1}} + C \vec{V}_{X_{k-1}} C^\top)^{-1} \quad (M.3)$$

$$F_{k-1} = I_{14} - \vec{V}_{X_{k-1}} C^\top G_{k-1} C. \quad (M.4)$$

Backward recursion for $k = K, K-1, \dots, 1$, with $\tilde{\xi}_{X_k} \in \mathbb{R}^{14}$ and $\tilde{W}_{X_k} \in \mathbb{R}^{14 \times 14}$, initialized with $\tilde{\xi}_{X_{K+1}} = 0_{14 \times 1}$ and $\tilde{W}_{X_{K+1}} = 0_{14 \times 14}$:

$$\tilde{\xi}_{X_k} = F_k^\top A^\top \tilde{\xi}_{X_{k+1}} - C^\top G_k (\vec{m}_{Y_k} - C \vec{m}_{X_k}) \quad (M.5)$$

$$\tilde{W}_{X_k} = F_k^\top A^\top \tilde{W}_{X_{k+1}} A F_k + C^\top G_k C. \quad (M.6)$$

Output: for $k \in \{1, 2, \dots, K\}$, the posterior means are

$$m_{W_k} = \vec{m}_{W_k} - \vec{V}_{W_k} D^\top B^\top \tilde{\xi}_{X_k} \quad (M.7)$$

$$m_{Y_k} = C(\vec{m}_{X_k} - \vec{V}_{X_k} \tilde{\xi}_{X_k}) \quad (M.8)$$

and for $\ell \in \{1, \dots, 6\}$, the posterior variance is

$$\sigma_{W_{k,\ell}}^2 = \left[\vec{V}_{W_k} - \vec{V}_{W_k} D^\top B^\top \tilde{W}_{X_k} B D \vec{V}_{W_k} \right]_{\ell,\ell}. \quad (M.9)$$

E. Iterative Augmented Kalman Estimation (IAKE)

Given the statistical model (28), the goal is to estimate w, y , and the unknown parameters θ (recall that the input sequence u is fully determined by w , see (19)). This statistical estimation problem is solved by an iterative algorithm, which repeats the following two steps for the iterations $i = 1, 2, 3, \dots$:

- 1) For fixed $\theta = \theta^{(i-1)}$, compute the posterior means $m_{W_k}^{(i)}$, $m_{Y_k}^{(i)}$, and the variances $(\sigma_{W_{k,\ell}}^2)^{(i)}$, for $k \in \mathcal{K}$ and $\ell \in \{1, \dots, 6\}$, of W_k and Y_k , respectively, using Table I.
- 2) From these means and variances, compute new parameters $\theta^{(i)}$ using Table II.

Note that Step 1 operates with a standard linear Gaussian model. In consequence, the required means and variances can be computed by Kalman-type recursions or, equivalently, by forward-backward Gaussian message passing, with a complexity that is linear in K . A preferred such algorithm is Modified Bryson–Frazier (MBF) message passing as in [29, Section V], which amounts to MBF smoothing [30] augmented with input estimation. The detailed algorithm is given in Table I. Note that the forward recursion is initialized with mean $\vec{m}_{X_0} = x_0$ and covariance matrix $\vec{V}_{X_0} = 0_{14 \times 14}$, where the initial state x_0 is derived from measurements and/or from the previous planning period.

TABLE II

UPDATE RULES FOR THE MEAN \vec{m}_Z AND THE VARIANCE $\vec{\sigma}_Z^2$ OF THE ‘‘PRIOR’’ $p(z) = \mathcal{N}(z; \vec{m}_Z, \vec{\sigma}_Z^2)$ FOR A CONSTRAINED SCALAR VARIABLE z .

	constraint	update rule
binary variable	$z \in \{a, b\}$	$\vec{\sigma}_Z^2 = \left[(\sigma_Z^2 + (m_Z - a)^2)^{-1} + (\sigma_Z^2 + (m_Z - b)^2)^{-1} \right]^{-1}$ $\vec{m}_Z = \vec{\sigma}_Z^2 \left[a (\sigma_Z^2 + (m_Z - a)^2)^{-1} + b (\sigma_Z^2 + (m_Z - b)^2)^{-1} \right]$
box constraint	$a \leq z \leq b$	$\vec{\sigma}_Z^2 = \gamma^{-1} \left(m_Z - a ^{-1} + m_Z - b ^{-1} \right)^{-1}$ $\vec{m}_Z = \gamma \vec{\sigma}_Z^2 \left(a m_Z - a ^{-1} + b m_Z - b ^{-1} \right)$
half-space constraint	$a \leq z$	$\vec{\sigma}_Z^2 = \gamma^{-1} m_Z - a $ $\vec{m}_Z = a + m_Z - a $
half-space constraint	$z \leq a$	$\vec{\sigma}_Z^2 = \gamma^{-1} m_Z - a $ $\vec{m}_Z = a - m_Z - a $

In Step 2, the unknown parameters θ are updated according to Table II, which is assembled from [21]–[23]. The table lists the update rules for the mean \vec{m}_Z and the variance $\vec{\sigma}_Z^2$ of a scalar ‘‘prior’’ $p(z) = \mathcal{N}(z; \vec{m}_Z, \vec{\sigma}_Z^2)$ expressing different constraints. The input to these update rules is the posterior mean m_Z and the posterior variance σ_Z^2 of Z as computed in Step 1.

Specifically, the parameters $\vec{m}_{W_{k,\ell}}^{(i)}$ and $(\vec{\sigma}_{W_{k,\ell}}^2)^{(i)}$ are updated according to the first row (‘‘binary variable’’) of Table II, with $m_Z = m_{W_{k,\ell}}^{(i)}$, $\sigma_Z^2 = (\sigma_{W_{k,\ell}}^2)^{(i)}$, $a = 0$ and $b = 1$, for $\ell \in \{1, \dots, 6\}$. The parameters $\vec{m}_{i_{c,n,k}}^{(i)}$ and $(\vec{\sigma}_{i_{c,n,k}}^2)^{(i)}$ are updated according to the second row (‘‘box constraint’’) of Table II, with $m_Z = m_{i_{c,n,k}}^{(i)}$, $a = -\delta_i$ and $b = \delta_i$, for $n \in \{a, b, c\}$. And finally, the parameters $\vec{m}_{v_{f,n,k}}^{(i)}$ and $(\vec{\sigma}_{v_{f,n,k}}^2)^{(i)}$ are also updated according to the second row (‘‘box constraint’’) of Table II, with $m_Z = m_{v_{f,n,k}}^{(i)}$, $a = -\delta_v$ and $b = \delta_v$, for $n \in \{a, b, c\}$. Note that all $m_{i_{c,n,k}}^{(i)}$ and $m_{v_{f,n,k}}^{(i)}$, $n \in \{a, b, c\}$, are determined by $m_{Y_k}^{(i)}$ (see (14)), and all $m_{W_{k,\ell}}^{(i)}$, $\ell \in \{1, \dots, 6\}$, are determined by $m_{W_k}^{(i)}$.

The algorithm terminates after some stopping criterion is satisfied (e.g., after some fixed number of iterations), and the final estimate of the input sequence is $\hat{u} = [\hat{u}_1 \ \dots \ \hat{u}_K]$, where \hat{u}_k is composed according to (19) with $w_k = m_{W_k}^{(i)}$. Note that \hat{u} is the solution of the constrained optimization problem (23) of the present planning period. Only the first M elements of \hat{u} are applied to the converter (see Section III-A and Fig. 2).

F. Constraint Satisfaction

In order to enforce the conditions (23b)–(23d), the three global parameters γ , s^2 , and r^2 must be chosen sufficiently large. Since it is not known a priori what ‘‘sufficiently large’’ means, it needs to be determined experimentally. In particular, when the algorithm of Section III-E stops, the

conditions (23b)–(23d) must be checked, and, if necessary, these parameters must be set to larger values.

For the numerical experiments in Section IV, the choice of γ is uncritical, and $\gamma = 100$ was used throughout. As to s^2 and r^2 , note from (23a) that increasing s^2 decreases the tracking accuracy while increasing r^2 allows more frequent input switches. In our numerical experiments, s^2 and r^2 were optimized manually.

G. Further Remarks

- The detailed working principle of the constraints used in Section III is beyond the scope of this paper. The reader is referred to [21]–[23].
- Inequality constraints as in the two bottom lines of Table II were not actually used in this paper, but may naturally occur in similar control problems.
- The only non-optimality in the proposed approach is how the discrete-level constraints (23b) are handled. The proposed algorithm will most likely terminate in a local, rather than the global, minimum of (23a). Computing the global minimum is infeasible for large K .
- The required number of iterations depends on K , but (empirically) saturates for $K \rightarrow \infty$ as detailed in Appendix A.

IV. PERFORMANCE EVALUATION

A. Figures of Merit

The total demand distortion (TDD) of an infinitely long single-phase current signal i is given by the RMS of $i - \check{i}$, where \check{i} is the fundamental component of i . Assuming that the rated current has the amplitude 1 per unit, the TDD for one phase is given by

$$\text{TDD} = \lim_{\tilde{K} \rightarrow \infty} \sqrt{\frac{1}{\tilde{K}} \sum_{k=1}^{\tilde{K}} (i_k - \check{i}_k)^2}, \quad (35)$$

TABLE III
PARAMETERS OF THE CONVERTER SYSTEM.

Symbol	Parameter	SI value	Per-unit value
\bar{S}_R	Rated apparent power	9 MVA	1
$V_{g,LL}$	Line-to-line grid voltage	3150 V	1.2247
I_R	Rated converter current	1650 A	0.7071
V_d	Dc-link voltage	4840 V	1.8818
L	Filter inductor	350 μ H	0.1
R	Filter inductor resistance	0.3 m Ω	0.00027
C	Filter capacitor	420 μ F	0.1455
R_C	Filter capacitor resistance	4 m Ω	0.0036
L_t	Transformer inductance	526.41 μ H	0.15
R_t	Transformer resistance	16.54 m Ω	0.015
L_g	Grid inductance	349.19 μ H	0.1
R_g	Grid resistance	10.97 m Ω	0.010
ω	Angular grid frequency	$2\pi 50$ rad s $^{-1}$	1

where, in practice, (35) is approximated by a finite \tilde{K} (that spans the whole simulation). The TDD of a three-phase current is then the mean value of the TDD of each phase.

The switching frequency in a fixed time interval centered at time step k can be approximated by counting the number of on-transitions in this interval and dividing the sum by the length of the interval. Recalling that an NPC converter has 12 semiconductor switches and that each switching transition incurs one on-transition, the switching frequency per semiconductor switch at time step k is then

$$f_{sw,k} \triangleq \frac{1}{12 \cdot 2\tilde{K}T_s} \sum_{i=-\tilde{K}}^{\tilde{K}} \|u_{k+i} - u_{k+i-1}\|_1, \quad (36)$$

where $2\tilde{K}T_s$ is the interval length with $\tilde{K} = 400$.

B. Parameters

Rated at 9 MVA, the converter's rated line-to-line voltage is 3150 V RMS and its rated current is 1650 A RMS. The angular grid frequency is $2\pi 50$ rad s $^{-1}$. Based on these quantities, a per-unit system is defined with the base values $V_B = \sqrt{2/3}V_{g,LL}$, $I_B = \sqrt{2}I_R$ and $\omega_B = \omega$. The values of all parameters are given in Table III. The control interval is $T_s = 25$ μ s.

C. Computational Burden

Fig. 5 shows the number of double-precision floating-point arithmetic operations (FLOP) as a function of the horizon length K and the number of iterations N_i . For short horizons K , the computational burden is significant, but it scales only linearly with K . The numbers were obtained using the performance analyzing tool `perf` under Linux.

Throughout the simulations, $N_i = 350$ was used. However, the algorithm can be stopped much earlier without sacrificing significant performance. An additional final rounding to the nearest integer in $\{-1, 0, 1\}$ may then be needed for each component of \hat{u}_k to ensure that $\hat{u}_k \in \{-1, 0, 1\}^3$.

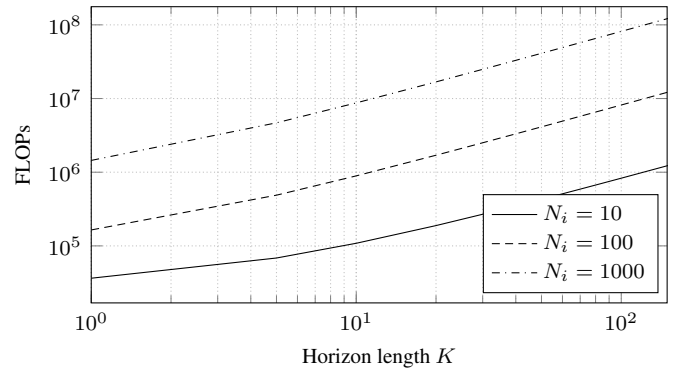


Fig. 5. Number of double-precision floating-point arithmetic operations (FLOPs) as a function of the horizon length K , for N_i iterations. The number of FLOPs scales linearly with K and N_i .

D. Steady-State Operation

The numerical results shown in Fig. 6 illustrate the steady-state operation of the converter at rated real power. The dashed lines in the first plot represent the reference grid current $\check{y}_{g,abc}$, whereas the solid lines represent the resulting grid current $i_{g,abc}$. The converter current $i_{c,abc}$ is shown in the second plot and the capacitor voltages $v_{f,abc}$ in the third plot. Finally, the three-phase switch positions u are illustrated in the last plot.

A switching frequency f_{sw} of approximately 317 Hz is obtained with $s^2 = 10^{-3}$ and $r^2 = 0.1$, where, as in (23a), s^2 penalizes deviations from the reference (grid) current and r^2 penalizes switching transitions in the input sequence (switch positions). At this switching frequency, a grid current TDD of 1.89% is achieved. The prediction horizon length was $K = 80$, and $M = 1$.

The harmonic amplitude spectrum of the three grid currents is shown in Fig. 7. Because the switching pattern is not periodic, the harmonic spectrum includes harmonics at frequencies that are non-integer multiples of the fundamental frequency of $f_1 = 50$ Hz. According to the IEEE 519 standard [31], non-integer harmonics are lumped to the closest integer harmonic by computing an equivalent RMS value. More specifically, the amplitude of the grid current harmonic at harmonic order n is calculated as $\sqrt{h_k^2 + \dots + h_\ell^2}$, where the square root comprises all spectral amplitude components h_k, \dots, h_ℓ in the frequency interval $[(n - 0.5)f_1, (n + 0.5)f_1]$, with $f_1 = \omega/(2\pi)$. The resulting amplitudes of the three grid current harmonics are shown in per unit in Fig. 7. As can be seen, the grid current meets the IEEE 519 standard, whose admissible bounds are depicted as solid black line. Note that different bounds apply for even and odd harmonics.

Furthermore, the controller seems to be quite robust to small changes in the grid parameters L_g and R_g (not known to the controller). For example, halving the grid inductance to $L'_g = 0.5 \cdot L_g = 0.05$ pu leads to a grid current TDD of 1.99% at a switching frequency f_{sw} of approximately 328 Hz, which is only marginally higher than the 1.89% obtained with known L_g .

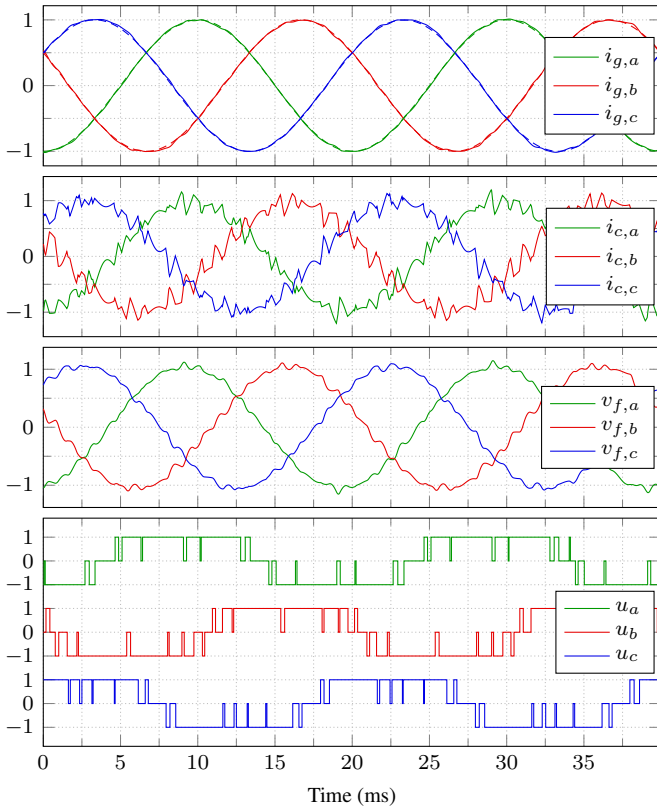


Fig. 6. Converter control operating in stationary mode with $K = 80$, $M = 1$, $s^2 = 10^{-3}$ and $r^2 = 0.1$, leading to a switching frequency of approximately $f_{sw} = 317$ Hz and a grid current TDD of 1.89%. The target (reference) current is shown as dashed lines in the top plot.

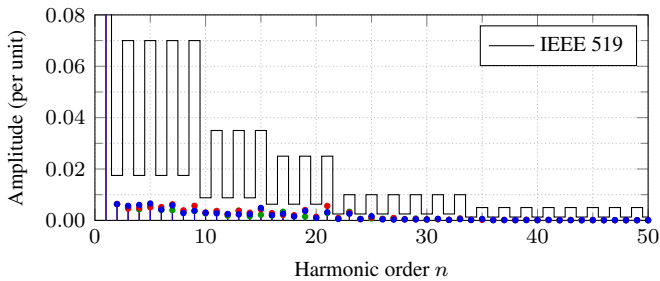


Fig. 7. Lumped harmonic amplitude spectrum of the three grid currents (the different phases are indicated by green, red and blue) for each harmonic integer order n . The admissible bounds of the IEEE 519 standard are depicted in black.

E. Transients

Fig. 8 shows the response of the controlled system to transients in the current reference. The current reference makes four steps: a first step (to 0.5 pu) at 6.75 ms, a second step (back to 1 pu) at 13.5 ms, a third step (to zero) at 23.25 ms, and a final step (back to 1 pu) 33.75 ms.

Such large steps in the grid current reference tend to incur high converter currents and/or capacitor voltages that might lead to a trip of the converter or even to it being damaged, cf. [7]. In order to avoid excessive converter currents and capacitor voltages, we impose bounds on both. In particular, we require $|i_{c,n,k}| \leq \delta_i$ and $|v_{c,n,k}| \leq \delta_v$, for $n \in \{a, b, c\}$ and $k \in \mathcal{K}$, with the bounds $\delta_i = 1.2$ pu and $\delta_v = 1.4$ pu, as

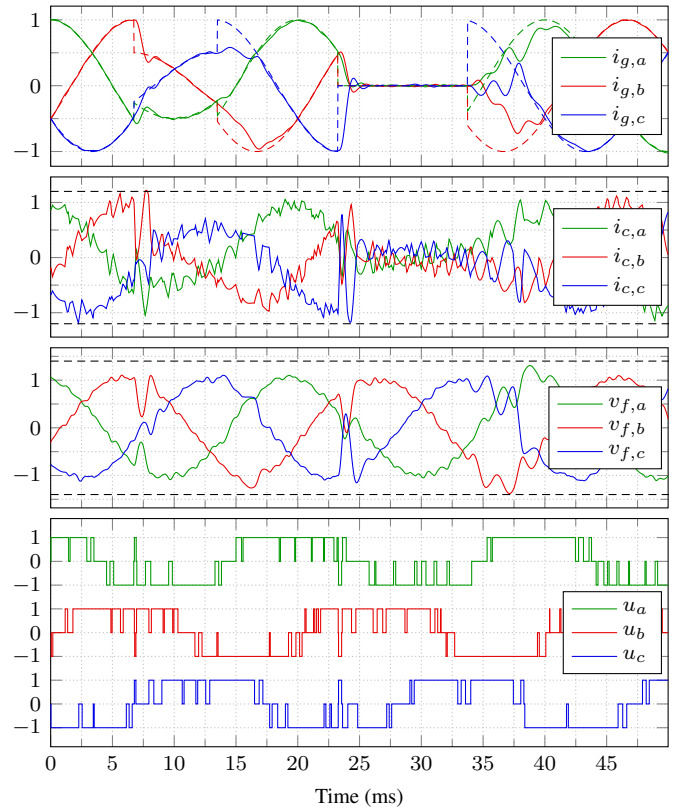


Fig. 8. Converter response to four steps in the reference grid current. The imposed state constraints $|i_{c,n}| \leq 1.2$ pu and $|v_{f,n}| \leq 1.4$ pu, with $n \in \{a, b, c\}$, are always met. The target (reference) current is shown as dashed lines in the top plot.

introduced in Section III-B. These bounds are illustrated as dashed black lines in the second and third plot of Fig. 8. (We also note here that the proposed control method is not limited to symmetric constraints: arbitrary half-space constraints can be imposed without increasing the computational complexity.)

It can be seen that the controller quickly regulates the grid currents to their corresponding references without violating any of the bounds. During the transients, the switching frequency temporarily increases for about 1 ms. As before, the presented numerical results are obtained with $s^2 = 10^{-3}$ and $r^2 = 0.1$, and $K = 80$ and $M = 1$.

F. Phase-to-Ground Fault

Finally, we consider a phase-to-ground fault. Operating at rated current, the grid voltage in phase a is set to zero at 10 ms. The time of the fault is indicated by a vertical dashed line in the first plot of Fig. 9.

In this particular example, we distinguish between a system model and a controller model. The system model (to which the control inputs are applied) is modified at 10 ms to represent the fault by setting $v_{g,a}(t) = 0$ for $t \geq 10$ ms. Because the controller is unaware of the fault, the controller model remains unaltered throughout the simulation. After each control period, the state vector of the system model is measured and used as initial state for the next control period.

As can be seen, the controller is capable of supplying a short-circuit current in phase a . Such a capability is often

$$C = \begin{bmatrix} 1 & -1 & 0 & 0 & 0 & 0 & 0 & 0 & 0 & 0 & 0 & 0 & 0 & 0 & 0 \\ 0 & 0 & 1 & -1 & 0 & 0 & 0 & 0 & 0 & 0 & 0 & 0 & 0 & 0 & 0 \\ 0 & 0 & 0 & 0 & 1 & -1 & 0 & 0 & 0 & 0 & 0 & 0 & 0 & 0 & 0 \\ 0 & 0 & 0 & 0 & 0 & 0 & 0 & 0 & 1 & 0 & 0 & 0 & 0 & 0 & 0 \\ 0 & 0 & 0 & 0 & 0 & 0 & 0 & 0 & 0 & 1 & 0 & 0 & 0 & 0 & 0 \\ 0 & 0 & 0 & 0 & 0 & 0 & 0 & 0 & 0 & 0 & 1 & 0 & 0 & 0 & 0 \\ 0 & 0 & 0 & 0 & 0 & 0 & 0 & 0 & 0 & 0 & 0 & 1 & 0 & 0 & 0 \\ 0 & 0 & 0 & 0 & 0 & 0 & 0 & 0 & 0 & 0 & 0 & -0.5 & 0.866 & 0 & 0 \\ 0 & 0 & 0 & 0 & 0 & 0 & 0 & 0 & 0 & 0 & 0 & -0.5 & -0.866 & 0 & 0 \\ 0 & 0 & 0 & 0 & 0 & 0 & 1 & 0 & 0 & 0 & 0 & 0 & 0 & 0 & 0 \\ 0 & 0 & 0 & 0 & 0 & 0 & -0.5 & 0.866 & 0 & 0 & 0 & 0 & 0 & 0 & 0 \\ 0 & 0 & 0 & 0 & 0 & 0 & -0.5 & -0.866 & 0 & 0 & 0 & 0 & 0 & 0 & 0 \end{bmatrix} \quad (41)$$

REFERENCES

- [1] S. Vazquez, J. Rodríguez, M. Rivera, L. G. Franquelo, and M. Norambuena, "Model predictive control for power converters and drives: Advances and trends," *IEEE Trans. Ind. Electron.*, vol. 64, no. 2, pp. 935–947, Feb. 2017.
- [2] P. Karamanakos, E. Liegmann, T. Geyer, and R. Kennel, "Model predictive control of power electronic systems: Methods, results, and challenges," *IEEE Open J. Ind. Appl.*, vol. 1, pp. 95–114, Aug. 2020.
- [3] S. Müller, U. Ammann, and S. Rees, "New modulation strategy for a matrix converter with a very small mains filter," in *Proc. IEEE Power Electron. Spec. Conf.*, Acapulco, Mexico, Jun. 2003.
- [4] J. Rodríguez, J. Pontt, C. Silva, M. Salgado, S. Rees, U. Ammann, P. Lezana, R. Huerta, and P. Cortés, "Predictive control of three-phase inverter," *IET Electronics Letters*, vol. 40, no. 9, pp. 561–563, Apr. 2004.
- [5] T. Geyer and D. E. Quevedo, "Performance of multistep finite control set model predictive control for power performance," *IEEE Trans. Power Electron.*, vol. 30, no. 3, pp. 1633–1644, Mar. 2015.
- [6] P. Karamanakos and T. Geyer, "Guidelines for the design of finite control set model predictive controllers," *IEEE Trans. Power Electron.*, vol. 35, no. 7, pp. 7434–7450, Jul. 2020.
- [7] T. Geyer, P. Karamanakos, and R. Kennel, "On the benefit of long-horizon direct model predictive control for drives with *LC* filters," in *Proc. IEEE Energy Convers. Congr. Expo.*, Pittsburgh, PA, USA, Sep. 2014.
- [8] U. Fincke and M. Pohst, "Improved methods for calculating vectors of short length in a lattice, including a complexity analysis," *Math. Comput.*, vol. 44, no. 170, pp. 463–471, Apr. 1985.
- [9] T. Geyer and D. E. Quevedo, "Multistep finite control set model predictive control for power electronics," *IEEE Trans. Power Electron.*, vol. 29, no. 12, pp. 6836–6846, Dec. 2014.
- [10] E. J. Fuentes, C. Silva, D. E. Quevedo, and E. I. Silva, "Predictive speed control of a synchronous permanent magnet motor," in *Proc. IEEE Int. Conf. Ind. Technol.*, Churchill, VIC, Australia, Feb. 2009.
- [11] P. Karamanakos, T. Geyer, and R. Kennel, "Constrained long-horizon direct model predictive control for power electronics," in *Proc. IEEE Energy Convers. Congr. Expo.*, Milwaukee, WI, USA, Sep. 2016.
- [12] G. S. Buja, "Optimum output waveforms in PWM inverters," *IEEE Trans. Ind. Appl.*, vol. 16, no. 6, pp. 830–836, Nov./Dec. 1980.
- [13] M. Dorfling, "Generalized model predictive pulse pattern control based on small-signal modelling," Ph.D. dissertation, Stellenbosch University, Stellenbosch, 2021.
- [14] S. Mariéthoz, A. Domahidi, and M. Morari, "High-bandwidth explicit model predictive control of electrical drives," *IEEE Trans. Ind. Appl.*, vol. 48, no. 6, pp. 1980–1992, Nov./Dec. 2012.
- [15] M. E. Tipping, "Sparse Bayesian learning and the relevance vector machine," *Journal of Machine Learning Research*, vol. 1, pp. 211–244, 2001.
- [16] M. E. Tipping and A. C. Faul, "Fast marginal likelihood maximisation for sparse Bayesian models," in *Proc. of the Ninth International Workshop on Artificial Intelligence and Statistics*, 2003, pp. 3–6.
- [17] D. P. Wipf and B. D. Rao, "Sparse Bayesian learning for basis selection," *IEEE Trans. Signal Process.*, vol. 52, no. 8, pp. 2153–2164, 2004.
- [18] D. P. Wipf and S. S. Nagarajan, "A new view of automatic relevance determination," in *Advances in Neural Information Processing Systems*, 2008, pp. 1625–1632.
- [19] I. Daubechies, R. DeVore, M. Fornasier, and C. S. Güntürk, "Iteratively reweighted least squares minimization for sparse recovery," *Communications on Pure and Applied Mathematics*, vol. 63, no. 1, pp. 1–38, 2010.
- [20] F. Bach, R. Jenatton, J. Mairal, and G. Obozinski, "Optimization with sparsity-inducing penalties," *Foundations and Trends in Machine Learning*, vol. 4, no. 1, pp. 1–106, 2012.
- [21] R. Keusch, H. Malmberg, and H.-A. Loeliger, "Binary Control and digital-to-analog conversion using composite NUV priors and iterative Gaussian message passing," in *Proc. IEEE Int. Conf. on Acoustics, Speech and Signal Processing (ICASSP)*, 2021, pp. 5330–5334.
- [22] R. Keusch and H.-A. Loeliger, "A binarizing NUV prior and its use for M-level control and digital-to-analog conversion," arXiv:2105.02599, 2021.
- [23] —, "Half-space and box constraints as NUV priors: First results," arXiv:2109.00036, 2021.
- [24] C. Hoffmann, A. Isler, and P. Rostalski, "A factor graph approach to parameter identification for affine LPV systems," in *American Control Conference (ACC)*, 2017, pp. 1910–1915.
- [25] C. Hoffmann and P. Rostalski, "Linear optimal control on factor graphs—a message passing perspective—," in *Proc. of the 20th IFAC World Congress*, 2017.
- [26] J. Watson, H. Abdulsamad, and J. Peters, "Stochastic optimal control as approximate input inference," in *Conference on Robot Learning*, PMLR, 2020, pp. 697–716.
- [27] L. Bruderer, *Input estimation and dynamical system identification: New algorithms and results*. Ph.D. dissertation, Nr. 22575, ETH Zurich.
- [28] W. Dueterhoeft, M. Schulz, and E. Clarke, "Determination of instantaneous currents and voltages by means of alpha, beta, and zero components," *AIEE Trans.*, vol. 70, no. 2, pp. 1248–1255, Jul. 1951.
- [29] H.-A. Loeliger, L. Bruderer, H. Malmberg, F. Wadehn, and N. Zalmai, "On sparsity by NUV-EM, Gaussian message passing, and Kalman smoothing," in *Information Theory and Applications Workshop (ITA)*, La Jolla, CA, USA, 2016, pp. 1–10.
- [30] G. J. Bierman, *Factorization Methods for Discrete Sequential Estimation*. Academic Press, 1977, vol. 128.
- [31] IEEE Std 519-1992, *IEEE Recommended Practices and Requirements for Harmonic Control in Electrical Power Systems*, New York, Apr. 1993.



Raphael Keusch earned his B.Sc. and M.Sc. degrees in electrical engineering from ETH Zurich, Switzerland, in 2014 and 2016, respectively. Following his master's degree, he joined Sensirion AG in Stäfa, Switzerland. In 2018, he returned to ETH Zurich to pursue research in the interdisciplinary fields of signal processing, optimization, and control, and completed his Ph.D. degree in 2022. Since 2023, he has been with Verity AG, Zurich, Switzerland.



Hans-Andrea Loeliger received both the Diploma in electrical engineering and the Ph.D. degree (1992) from ETH Zurich, Switzerland. From 1992 to 1995, he was with Linköping University, Linköping Sweden. From 1995 to 2000, he was a technical consultant and coowner of a consulting company. Since 2000, he has been a Professor with the Department of Information Technology and Electrical Engineering of ETH Zurich, Switzerland. His research interests have been in the broad areas of signal processing,

machine learning, information theory, communications, error correcting codes, electronic circuits, quantum systems, and neural computation. He is a Fellow of the IEEE.



Tobias Geyer received the Dipl.-Ing. degree in electrical engineering, the Ph.D. in control engineering and the Habilitation degree in power electronics from ETH Zurich in the years 2000, 2005 and 2017, respectively.

After his Ph.D., he spent three years at GE Global Research, Munich, Germany, three years at the University of Auckland, Auckland, New Zealand, and eight years at ABB's Corporate Research Centre, Baden-Dättwil, Switzerland. In 2020, he joined ABB's Medium-Voltage Drive division as R&D platform manager of the ACS6080. In 2022, he became a Corporate Executive Engineer. He has been an extraordinary Professor at Stellenbosch University, Stellenbosch, South Africa, since 2017.

He is the author of more than 40 patent families, 160 publications and the book "Model predictive control of high power converters and industrial drives" (Wiley, 2016). He teaches a regular course on model predictive control at ETH Zurich. His research interests include medium-voltage and low-voltage drives, utility-scale power converters, optimized pulse patterns and model predictive control.

Dr. Geyer received the PELS Modeling and Control Technical Achievement Award in 2022, the Semikron Innovation Award in 2021, and the Nagamori Award in 2021. He also received two Prize Paper Awards of IEEE Transactions and three Prize Paper Awards at IEEE conferences. He is a former Associate Editor of the Transactions on Industry Applications (from 2011 until 2014) and the Transactions on Power Electronics (from 2013 until 2019). He was an International Program Committee Vice Chair of the IFAC conference on Nonlinear Model Predictive Control in Madison, WI, USA, in 2018. Dr. Geyer is a former Distinguished Lecturer of the Power Electronics Society (from 2020 until 2023). He is a Fellow of the IEEE.